Physics Letters A 378 (2014) 348–357

Contents lists available at ScienceDirect

Physics Letters A

www.elsevier.com/locate/pla

A new car-following model with two delays

Lei Yu [a,*], Zhong-ke Shi [a], Tong Li [b]

[a] College of Automation, Northwestern Polytechnical University, Xi'an, ShaanXi, China
[b] Department of Mathematics, University of Iowa, Iowa City, IA, USA

ARTICLE INFO

Article history:
Received 13 September 2013
Received in revised form 23 November 2013
Accepted 25 November 2013
Available online 27 November 2013
Communicated by C.R. Doering

Keywords:
Car-following model
Two time delays
Stability condition
mKdV equation
Traffic jams

ABSTRACT

A new car-following model is proposed by taking into account two different time delays in sensing headway and velocity. The effect of time delays on the stability analysis is studied. The theoretical and numerical results show that traffic jams are suppressed efficiently when the difference between two time delays decreases and those can be described by the solution of the modified Korteweg–de Vries (mKdV) equation. Traffic flow is more stable with two delays in headway and velocity than in the case with only one delay in headway. The impact of local small disturbance to the system is also studied.

1. Introduction

To gain a good understanding of complex behavior of the vehicular traffic flow, numerous mathematical traffic models were developed. Car-following models describe the traffic flow by individual driver behavior in which drivers follow the leaders in the traffic stream. Although car-following models have been studied for more than half a century, its importance has been understood further in some systems, such as Adaptive Cruise Control (ACC) [1]. Here we give some typical car-following models, such as the optimal velocity (OV) model introduced by Bando et al. [2], a generalized force (GF) model with a velocity difference term added into the OV model proposed by Helbing and Tilch [3] and a full velocity difference (FVD) model developed by Jiang et al. [4]. Although the OV model is shown to have the universal structure in describing many properties of the traffic flow, many approaches to extend the model toward more realistic traffic models have been pursued. The calibration of the OV model using the empirical data shows that high acceleration or unrealistic deceleration occurs in the OV model [3]. Comparing with the OV model and the GF model, the FVD model considers more aspects in car-following process and is more realistic. In addition, two different deterministic microscopic traffic flow models were introduced in the context of Kerner's three-phase traffic theory [5]. There are some other kinds of traffic models such as the cellular automaton models [6–12] and the continuum models [13–20].

Based on these car-following models, many researchers investigated various properties of the traffic flow, such as the nonlinear waves. Komatsu and Sasa [21] analyzed the OV model and derived the modified Korteweg–de Vries (mKdV) equation to describe traffic jams as kink density wave which is the solution of the mKdV equation. Muramatsu and Nagatani [22] derived the Korteweg–de Vries (KdV) equation from the OV model and described traffic jams as soliton density waves which is the solution of the KdV equation. Ou et al. [23] studied the density waves of the FVD model. Yu et al. [24] proposed an extended FVD model by considering the headway of arbitrary number of cars and derived the mKdV equation. Nagatani [25] presented detailed method about how to obtain the nonlinear wave equations from car-following models.

In the car-following models, many parameters appear to describe the physical conditions of roads, mechanical properties of vehicles, states of drivers, traffic laws, etc. [26]. Among these parameters, time delay is a critical one which has been recognized in the traffic studies since 1958 [27–35]. Bando et al. [28] demonstrated that in the OV model delay times of vehicles coming from the dynamical equation of motion of the OV model explain the order of delay times observed in actual traffic flows without introducing explicit delay times. They found that in most of the situation for which an effective delay time can be made a reasonable definition. Davis [29] posed a traffic model with a delay time due to driver's reaction-time. It consists of a system of delay differential equations and is a variation of the OV model. Orosz et al. [30, 31] investigated the local and global bifurcations of the OV model with reaction-time delay of drivers. Analytical stability study of some deterministic car following models under time-delay influences were presented and various case studies were demonstrated

* Corresponding author. Tel.: +86 15339260284.
E-mail address: yuleijk@126.com (L. Yu).

0375-9601/$ – see front matter
http://dx.doi.org/10.1016/j.physleta.2013.11.030

in Ref. [32]. Kesting et al. [33] investigated two causes for the instability of the traffic flow: the time lag caused by finite accelerations of the vehicles and the delay caused by the finite reaction times of the drivers. A car-following model was proposed by taking into account the delay of the driver's response in sensing headway and the delay plays an important role in jamming transition [34,35]. Density waves were investigated analytically and numerically in the optimal velocity model with reaction-time delay of drivers [36].

It is known that time delays mainly originated from the time needed by drivers in sensing stimulus, making decision and performing control actions against real-time variations in the dynamical traffic flow. Some papers study only the driver's time delay in sensing headway. In general, the time delays in sensing headway and in sensing velocity are different [37]. But for the sake of simplicity, the different kinds of time delays are considered to be equal to each other or to be zero. We are interested in the variation of stability condition and jamming transition caused by the two different time delays.

In this paper, we propose a new car-following model by taking into account two different time delays in sensing headway and velocity in Section 2. The delays may have an important effect upon the property of the traffic flow, especially the stability condition. A thorough stability analysis is given to study the effects of time delays in Section 3. The evolution of traffic jams which is described by the mKdV equation is given in Section 4. The numerical simulations are presented in Section 5.

2. The model

The dynamical equation of the nth vehicle of the FVD model [4] is given by

$$\frac{\mathrm{d}^2x_n(t)}{\mathrm{d}t^2} = a\big[V\big(\Delta x_n(t)\big) - v_n(t)\big] + \lambda\Delta v_n(t), \tag{1}$$

where $x_n(t)$ is the position of the nth vehicle at time t, $v_n(t)$ is the velocity of the nth vehicle at time t, $\Delta x_n = x_{n+1} - x_n$ is the headway between two successive vehicles of the $(n+1)$th and the nth vehicles, $\Delta v_n = v_{n+1} - v_n$ is the velocity difference (i.e., the relative velocity), $V(\Delta x_n(t))$ is the optimal velocity function, $a > 0$ is the sensitivity and λ is the coefficient of the relative velocity. In this case each driver's response to the stimulus from the vehicle ahead of the driver is instantaneous.

The current paper is concerned with an extended FVD model which contains two delays one in sensing headway and the other in sensing relative velocity. The acceleration of the nth vehicle is given by a delay differential equation (DDE)

$$\frac{\mathrm{d}^2x_n(t)}{\mathrm{d}t^2} = a\big[V\big(\Delta x_n(t-\tau_1)\big) - v_n(t-\tau_2)\big] + \lambda\Delta v_n(t-\tau_2), \tag{2}$$

where $\tau_1, \tau_2 \geqslant 0$ are introduced to represent the delays of in headway and in relative velocity. For simplicity, τ_1 and τ_2 are assumed to be the same for all drivers. The limit case of $\tau_1 = \tau_2 = 0$ is the original FVD model. We call Eq. (2) FVD model with delays (FVD-Ds model).

The optimal velocity function V is given by [2]

$$V\big(\Delta x_n(t)\big) = \frac{v_{\max}}{2}\big[\tanh\big(\Delta x_n(t) - h_c\big) + \tanh(h_c)\big], \tag{3}$$

where h_c is the safety distance and $v_{\max}$ is the maximum velocity. The optimal velocity function is a monotonically increasing function of the headway and has an upper bound, i.e., the maximal velocity. When the headway is less than the safety distance, the vehicle reduces its velocity to prevent from crashing into the preceding vehicle. On the other hand, if the headway is larger than the safety distance, it increases toward the maximal velocity. The optimal velocity function given by Eq. (3) has a turning point (inflection point) at $\Delta x_n = h_c$, that is,

$$V''(h_c) = \left.\frac{\mathrm{d}^2V(\Delta x_n)}{\mathrm{d}\Delta x_n^2}\right|_{\Delta x_n = h_c} = 0.$$

It is very important that the optimal velocity has an inflection point in deriving the mKdV equation of FVD-Ds model which gives the kink–antikink solutions to describe traffic jams.

3. Linear stability analysis

In this section, a thorough stability analysis is given to study the effect of the two delays on the stability condition of the FVD-Ds model. The procedure is similar to that of Ref. [2]. Stability of a uniform traffic flow is considered. The uniform traffic flow is defined by such a state that all cars move with identical headway h and optimal velocity $V(h)$. Then the solution $x_n^{(0)}(t)$ representing the uniform steady state of the FVD-Ds model can be written as

$$x_n^{(0)}(t) = hn + V(h)t. \tag{4}$$

Let $x_n(t)$ be a small deviation from the uniform steady state $x_n^{(0)}(t)$: $x_n(t) = x_n^{(0)}(t) + y_n(t)$ where $y_n(t)$ is the small deviation. Then the linearized equation for $y_n(t)$ is obtained from the FVD-Ds model

$$\frac{\mathrm{d}^2y_n(t)}{\mathrm{d}t^2} = a\left[V'(h)\Delta y_n(t-\tau_1) - \frac{\mathrm{d}y_n(t-\tau_2)}{\mathrm{d}t}\right] + \lambda\frac{\mathrm{d}\Delta y_n(t-\tau_2)}{\mathrm{d}t}, \tag{5}$$

where $V'(h)$ is the derivative of optimal velocity function $V(\Delta x_n(t))$ at $\Delta x_n(t) = h$ and $\Delta y_n(t) = y_{n+1}(t) - y_n(t)$. By expanding $y_n(t) \propto \exp(\mathrm{i}kn + zt)$, the following equation of z is obtained from Eq. (5)

$$z^2 + \big[a\mathrm{e}^{-z\tau_2} - \lambda\mathrm{e}^{-z\tau_2}\big(\mathrm{e}^{\mathrm{i}k} - 1\big)\big]z - aV'(h)\mathrm{e}^{-z\tau_1}\big(\mathrm{e}^{\mathrm{i}k} - 1\big) = 0. \tag{6}$$

Here we derive the long-wave expansion of z which is determined by the order of $\mathrm{i}k$ around $\mathrm{i}k \approx 0$ [25]. By expanding $z = z_1(\mathrm{i}k) + z_2(\mathrm{i}k)^2 + \cdots$ and inserting it into Eq. (6), the first- and the second-order terms of $\mathrm{i}k$ are collected

$$z_1 = V'(h),$$
$$z_2 = \left(\frac{\lambda}{a} + \frac{1}{2}\right)V'(h) + \left(\tau_2 - \tau_1 - \frac{1}{a}\right)V'(h)^2. \tag{7}$$

If z_2 is negative, the uniform steady state becomes unstable for long-wavelength modes. If z_2 is positive, the uniform steady state becomes stable. Thus, for small disturbances of long wavelength, the uniform traffic flow is stable if

$$\frac{2(V'(h) - \lambda)}{a} < 1 - 2V'(h)(\tau_1 - \tau_2). \tag{8}$$

The neutral stability condition is given by

$$a_s = \frac{2(V'(h) - \lambda)}{1 - 2V'(h)(\tau_1 - \tau_2)}. \tag{9}$$

When $\tau_1 = \tau_2 \geqslant 0$, the stability condition Eq. (9) is simply the same as the one in the FVD model in Ref. [4].

In Fig. 1, the values of parameters are $v_{\max} = 3.0$ and $h_c = 4.0$. Fig. 1(a1) and (a2) show the spinodal lines (also called the neutral stability lines) of the FVD-Ds model by using different line

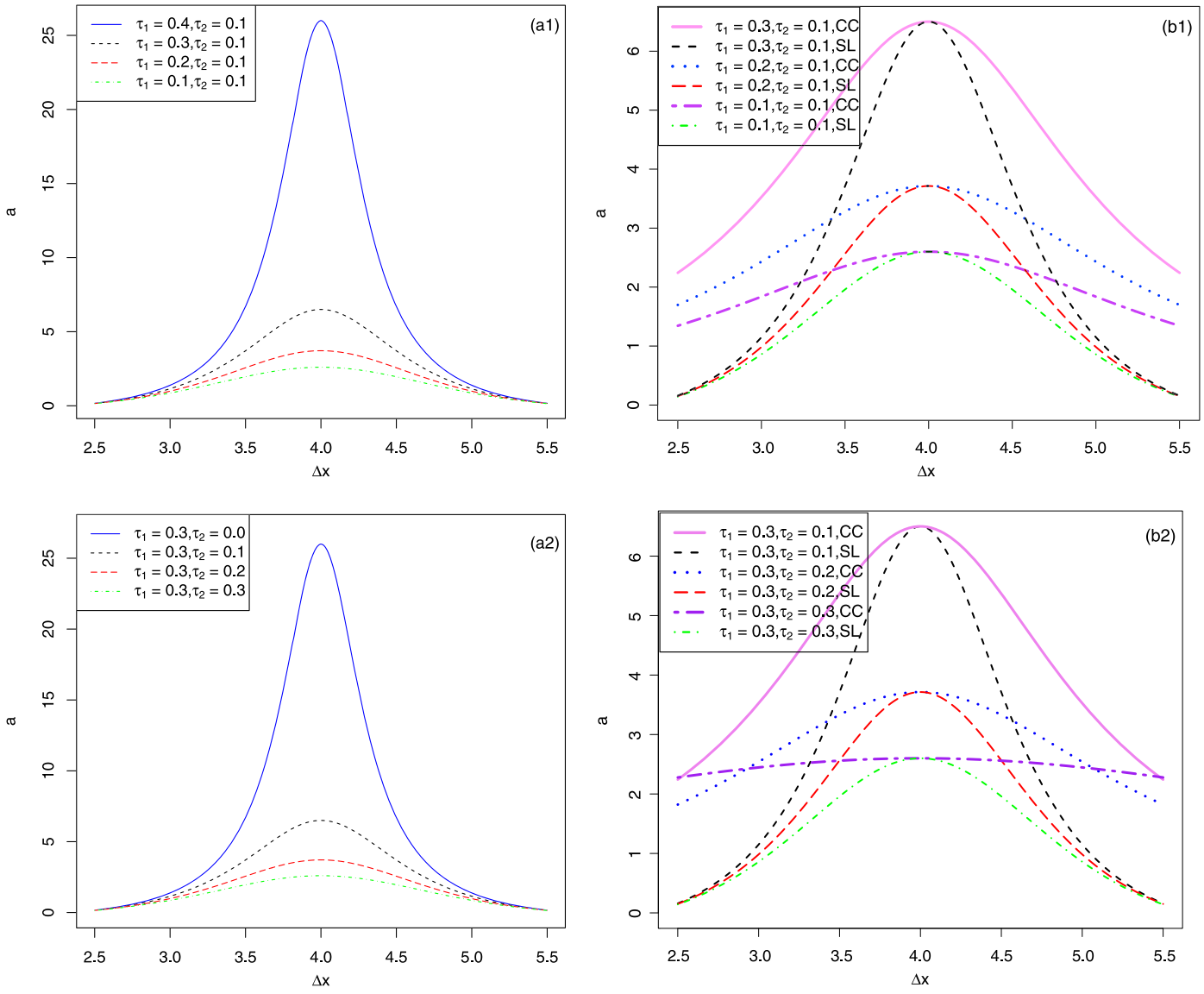

Fig. 1. (a1), (a2): the spinodal line of FVD-Ds model; (b1), (b2): phase diagram of FVD-Ds model.

styles for different values of τ_1 and τ_2 where Δx is the headway and a is the sensitivity. From Fig. 1(a1) and (a2), we can find that the curves coincide when the difference between τ_1 and τ_2 is equal and the spinodal lines increase with increasing the difference between τ_1 and τ_2. The apex of each curve is the critical point (h_c, a_c) and $a_c = (v_{\max} - 2\lambda)/(1 - v_{\max}(\tau_1 - \tau_2))$. When $\tau_1 = \tau_2 \geqslant 0$, its spinodal line coincides with those of $\tau_1 = \tau_2 = 0.1$ or 0.3 because their differences are all 0. When $\tau_1 = \tau_2 = 0$, the spinodal line and the critical point agree with those of the FVD model [4]. From Fig. 1(a2), the spinodal lines for various values of τ_2 are shown from the top down with the same value of τ_1.

Fig. 1(b1) and (b2) show the phase diagrams of the FVD-Ds model with different τ_1 and τ_2 where the word "CC" represents the coexisting curve and the word "SL" represents the spinodal line in the legend. Comparing with Fig. 1(a1) and (a2), Fig. 1(b1) and (b2) are the corresponding coexisting curve of each pair of τ_1 and τ_2 and the drawing of partial enlargements of Fig. 1(a1) and (a2), respectively. The coexisting curve, the spinodal line and the critical point are similar to the conventional gas–liquid phase transition. Three regions in the traffic flow are distinguished: the stable region which is out of the coexisting curve, the metastable region which is between the coexisting curve and the spinodal line and the unstable region which is within the spinodal line. From Fig. 1(b1) and (b2), the traffic flow is more stable with decreasing the difference between τ_1 and τ_2. Comparing with other cases of Fig. 1(a2), we find that the traffic flow is more unstable when $\tau_1 = 0.3$ and $\tau_2 = 0.0$. The traffic flow is more stable with two delays in headway and in velocity than in the case with only one delay in headway.

In Section 4, we will see that traffic jams appear as the kink–antikink density waves as the solutions of the mKdV equation only near the critical point in the unstable region by using the reductive perturbation method. In Section 5, numerical simulations will be given to investigate the impact of small perturbations to the traffic flow with different time delays. Those results agree with Figs. 1(a1), (a2), (b1) and (b2).

4. The MKdV equation

To derive the mKdV equation describing the kink–antikink density wave from the FVD-Ds model near the critical point, we use the reductive perturbation method introduced in [21].

For later convenience, the FVD-Ds model can be rewritten as

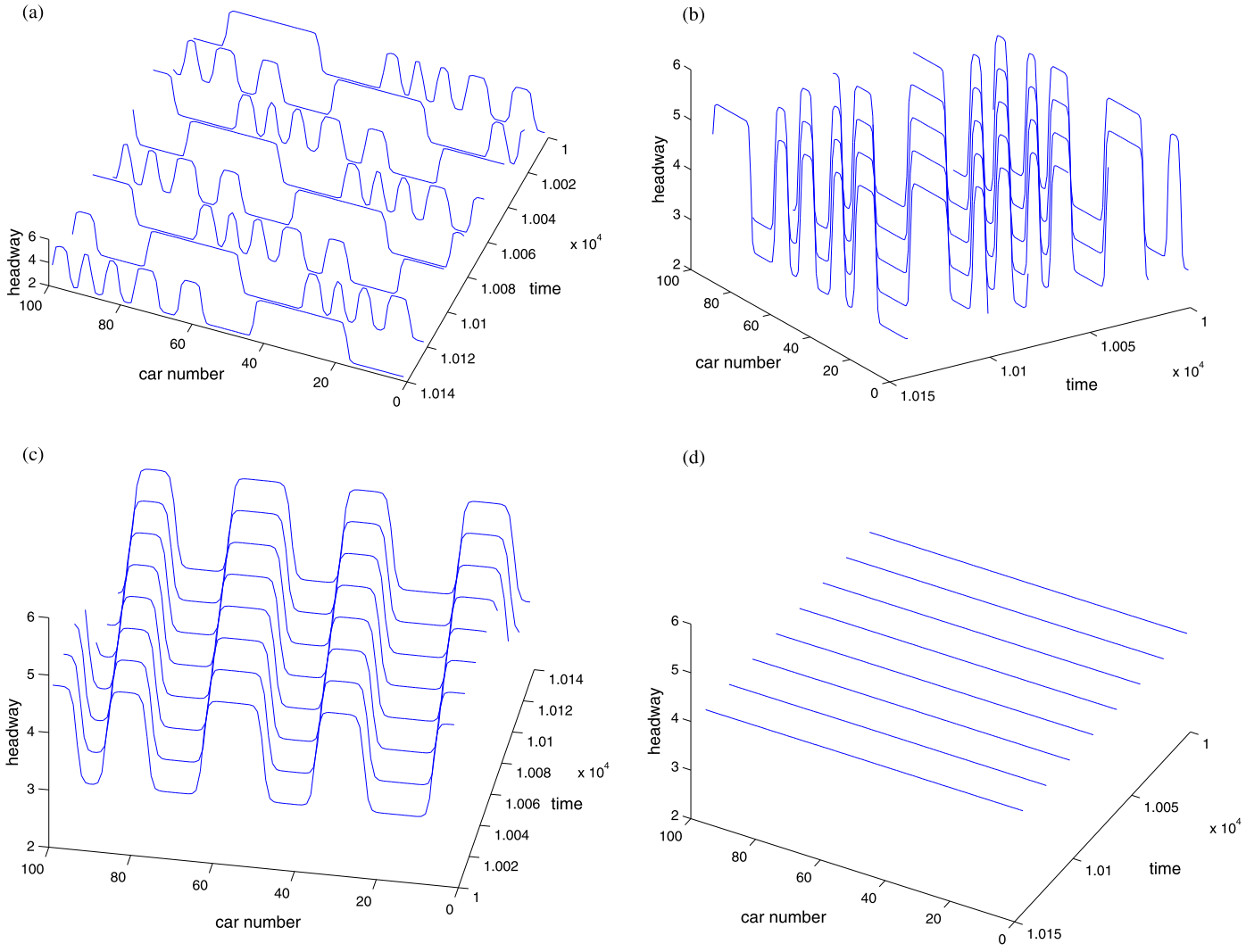

Fig. 2. Space–time evolution of the headway with different τ_1 and $\tau_2 = 0.1$ after $t = 10\,000$ ($a = 2.95$).

$$\frac{\mathrm{d}^2\Delta x_n(t)}{\mathrm{d}t^2} = a\big[V\big(\Delta x_{n+1}(t-\tau_1)\big) - V\big(\Delta x_n(t-\tau_1)\big) - \Delta v_n(t-\tau_2)\big] + \lambda\big[\Delta v_{n+1}(t-\tau_2) - \Delta v_n(t-\tau_2)\big]. \tag{10}$$

Now we consider long-wavelength modes in the unstable traffic flow region. We apply the reductive perturbation method to Eq. (10) by performing the long-wave expansion as following. We introduce slow scales for space variable n and time variable t and define slow variables X and T, for $0 < \varepsilon \ll 1$

$$X = \varepsilon(n + bt), \qquad T = \varepsilon^3 t, \tag{11}$$

where b is a constant to be determined. We set the headway as

$$\Delta x_n(t) = h_c + \varepsilon R(X, T). \tag{12}$$

The critical point in Fig. 1 is the turning point (infection point) where $V''(h_c) = 0$. The critical point is necessary to obtain the mKdV equation which has the kink–antikink density wave solution representing traffic jams.

By inserting Eq. (11) and Eq. (12) into Eq. (10) and expanding the result to the fifth order of ε, the following nonlinear partial differential equation is obtained

$$\varepsilon^2 a(b - c_1)\partial_X R + \varepsilon^3\left[(1 - a\tau_2)b^2 - \lambda b - \frac{a(1 - 2b\tau_1)}{2}c_1\right]\partial_X^2 R + \varepsilon^4\left[a\partial_T R - \left(\frac{(1 - b\tau_1)^3 + (b\tau_1)^3}{6}ac_1 + \frac{b\lambda(1 - 2b\tau_2)}{2} - \frac{ab^3\tau_2^3}{2}\right)\partial_X^3 R - \frac{ac_3}{6}\partial_X R^3\right] + \varepsilon^5\left[\big(2b(1 - a\tau_2) + ac_1\tau_1 - \lambda\big)\partial_X\partial_T R - \left(\frac{(1 - b\tau_1)^4 - (b\tau_1)^4}{24}ac_1 + \frac{(1 - b\tau_2)^3 + (b\tau_2)^3}{6}\lambda b + \frac{ab^4\tau_2^3}{6}\right)\partial_X^4 R - \frac{a(1 - 2b\tau_1)}{12}c_3\partial_X^2 R^3\right] = 0, \tag{13}$$

where $c_1 = V'(h_c) = \mathrm{d}V/\mathrm{d}\Delta x|_{\Delta x = h_c}$ and $c_3 = V'''(h_c) = \mathrm{d}^3V/\mathrm{d}(\Delta x)^3|_{\Delta x = h_c}$ are constants.

Let

$$\frac{a_c}{a} = 1 + \varepsilon^2 \tag{14}$$

for a near the critical value a_c. Taking $b = c_1$ and substituting Eq. (14) into Eq. (13), the second- and the third-order terms of ε in Eq. (13) can be eliminated and Eq. (13) can be rewritten as

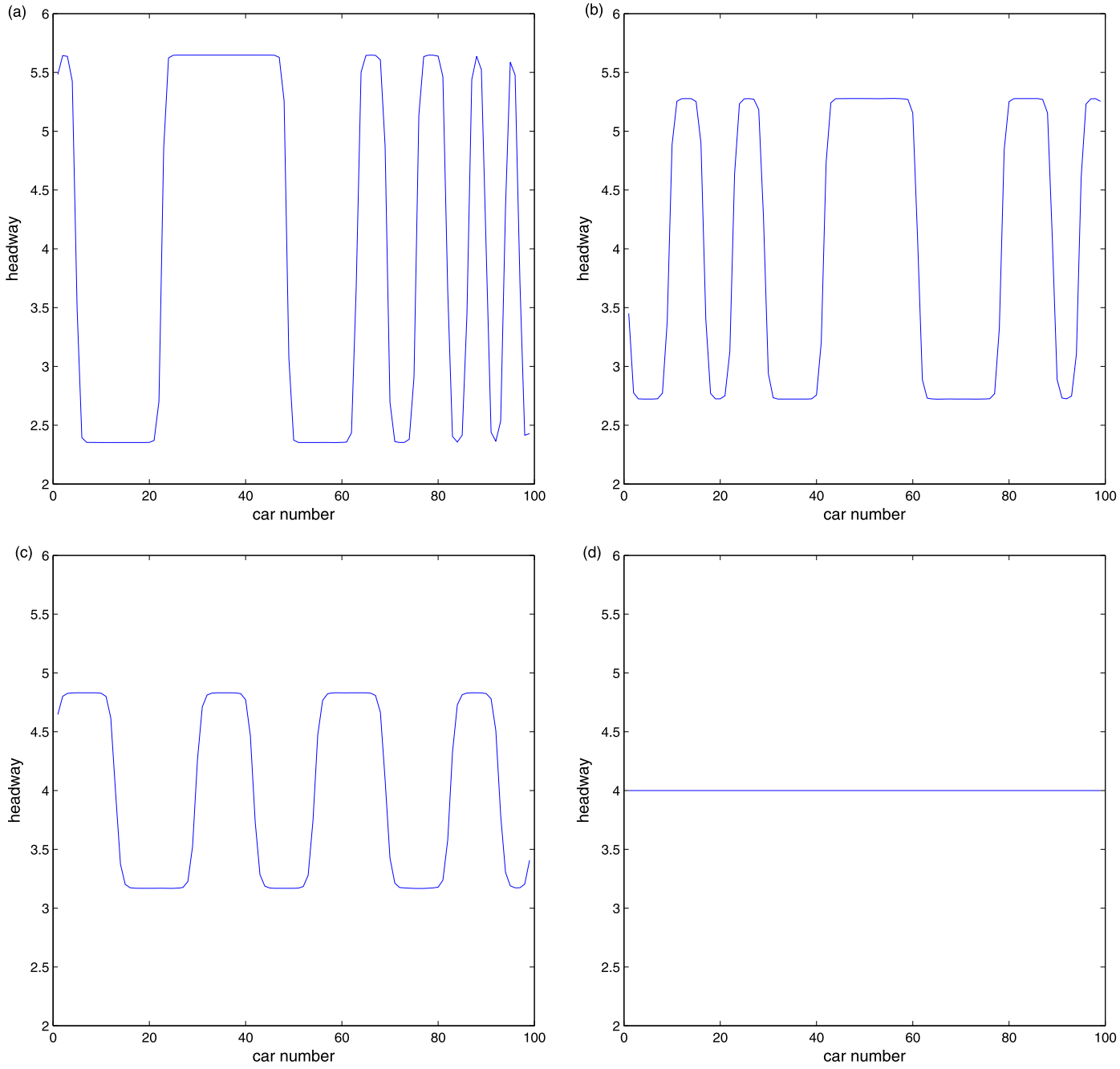

Fig. 3. Headway profile of the density wave at $t = 10080$ correspond to Fig. 2, respectively.

$$\varepsilon^4\left[\partial_T R - g_1\partial_X^3 R + g_2\partial_X R^3\right] + \varepsilon^5\left[g_3\partial_X^2 R + g_4\partial_X^2 R^3 + g_5\partial_X^4 R\right] = 0, \tag{15}$$

where

$$g_1 = \frac{(1-c_1\tau_1)^3 + (c_1\tau_1)^3}{6}c_1 + \frac{1-2c_1\tau_2}{2a}c_1\lambda - \frac{(c_1\tau_2)^3}{2},$$

$$g_2 = -\frac{c_3}{6},$$

$$g_3 = \frac{1-2c_1\tau_1}{2}c_1 + \tau_2 c_1^2,$$

$$g_4 = \left(\frac{c_1(1-a\tau_2)}{3a} + \frac{c_1\tau_1}{6} - \frac{1-2c_1\tau_1}{12} - \frac{\lambda}{6a}\right)c_3,$$

$$g_5 = \left(\frac{(1-c_1\tau_1)^3 + (c_1\tau_1)^3}{6}c_1 + \frac{1-2c_1\tau_2}{2a}c_1\lambda - \frac{(c_1\tau_2)^3}{2}\right)\left(c_1(\tau_1 - 2\tau_2) + \frac{2c_1-\lambda}{a}\right) - \frac{(1-c_1\tau_1)^4 - (c_1\tau_1)^4}{24}c_1 - \frac{(1-c_1\tau_2)^3 - (c_1\tau_2)^3}{6a}\lambda c_1 - \frac{c_1^4\tau_2^3}{6}.$$

Because we adopt the explicit form of the optimal velocity function (3), we calculate that $c_1 = v_{\max}/2$ and $c_3 = -v_{\max}$ at the critical point.

In order to derive the standard mKdV equation with higher order correction, we make the following transformation in Eq. (15)

$$T = \frac{1}{g_1}T_m, \qquad R = \sqrt{\frac{g_1}{g_2}}R_m. \tag{16}$$

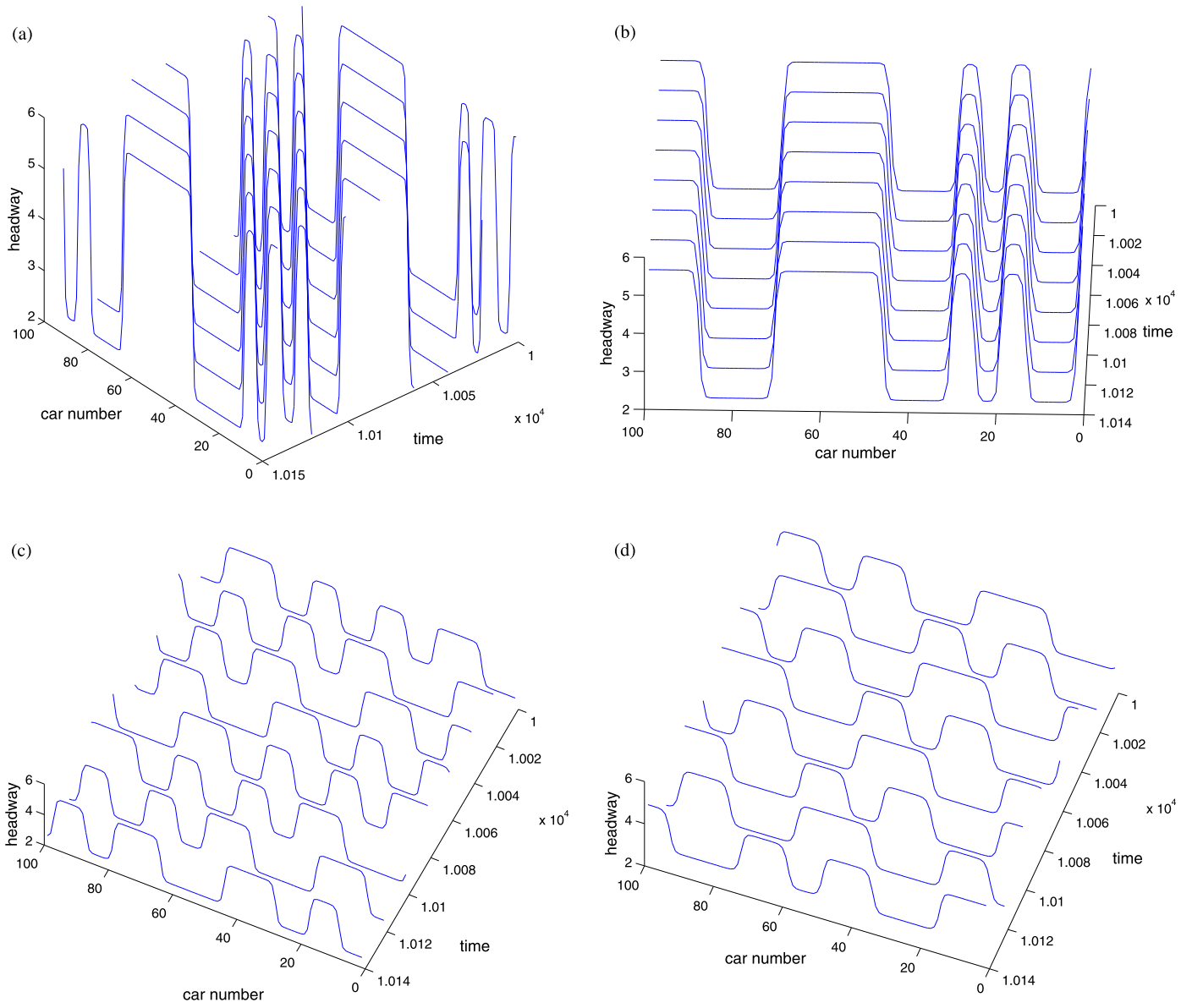

Fig. 4. Space–time evolution of the headway with different τ_1 and $\tau_2 = 0.1$ after $t = 10\,000$ ($a = 2.0$).

Then we obtain the standard mKdV equation with higher order correction terms

$$\partial_{T_m} R_m - \partial_X^3 R_m + \partial_X R_m^3 + \frac{\varepsilon}{g_1}\left[g_3 \partial_X^2 R_m + \frac{g_1 g_4}{g_2}\partial_X^2 R_m^3 + g_5 \partial_X^4 R_m\right] = 0. \tag{17}$$

If we ignore the $O(\varepsilon)$ terms in Eq. (17), it is just the mKdV equation with the kink–antikink solution

$$R_{m0}(X, T_m) = \sqrt{B}\tanh\sqrt{\frac{B}{2}}(X - BT_m). \tag{18}$$

Amplitude B of kink–antikink solutions of the mKdV equation in Eq. (18) is a free parameter. The $O(\varepsilon)$ term in Eq. (17) gives the condition on selecting a unique member from the continuous family of mKdV solitons. In order to determine the value of B for the kink–antikink solution (18), the solvability condition

$$\left(R_{m0}, M[R_{m0}]\right) \equiv \int_{-\infty}^{\infty} \mathrm{d}X\, R_{m0} M[R_{m0}] = 0, \tag{19}$$

where $M[R_{m0}]$ is the $O(\varepsilon)$ term in Eq. (17), must be satisfied. By performing the integration in Eq. (19), we obtain the value of propagation velocity B for the kink–antikink solution as follows

$$B = \frac{5g_2 g_3}{2g_2 g_5 - 3g_1 g_4}, \tag{20}$$

which is the same as the one in Ref. [38]. Substituting Eq. (16) into Eq. (18), we obtain the solution of the mKdV equation

$$R(X, T) = \sqrt{\frac{g_1 B}{g_2}}\tanh\left[\sqrt{\frac{B}{2}}(X - Bg_1 T)\right]. \tag{21}$$

We also obtain the kink–antikink solution of the headway from Eq. (12)

$$\Delta x_n(t) = h_c + \sqrt{\frac{g_1 B}{g_2}\left|\frac{a_c}{a} - 1\right|} \times \tanh\left\{\sqrt{\frac{B}{2}\left|\frac{a_c}{a} - 1\right|}\left(n + c_1 t - Bg_1\left|\frac{a_c}{a} - 1\right| t\right)\right\}. \tag{22}$$

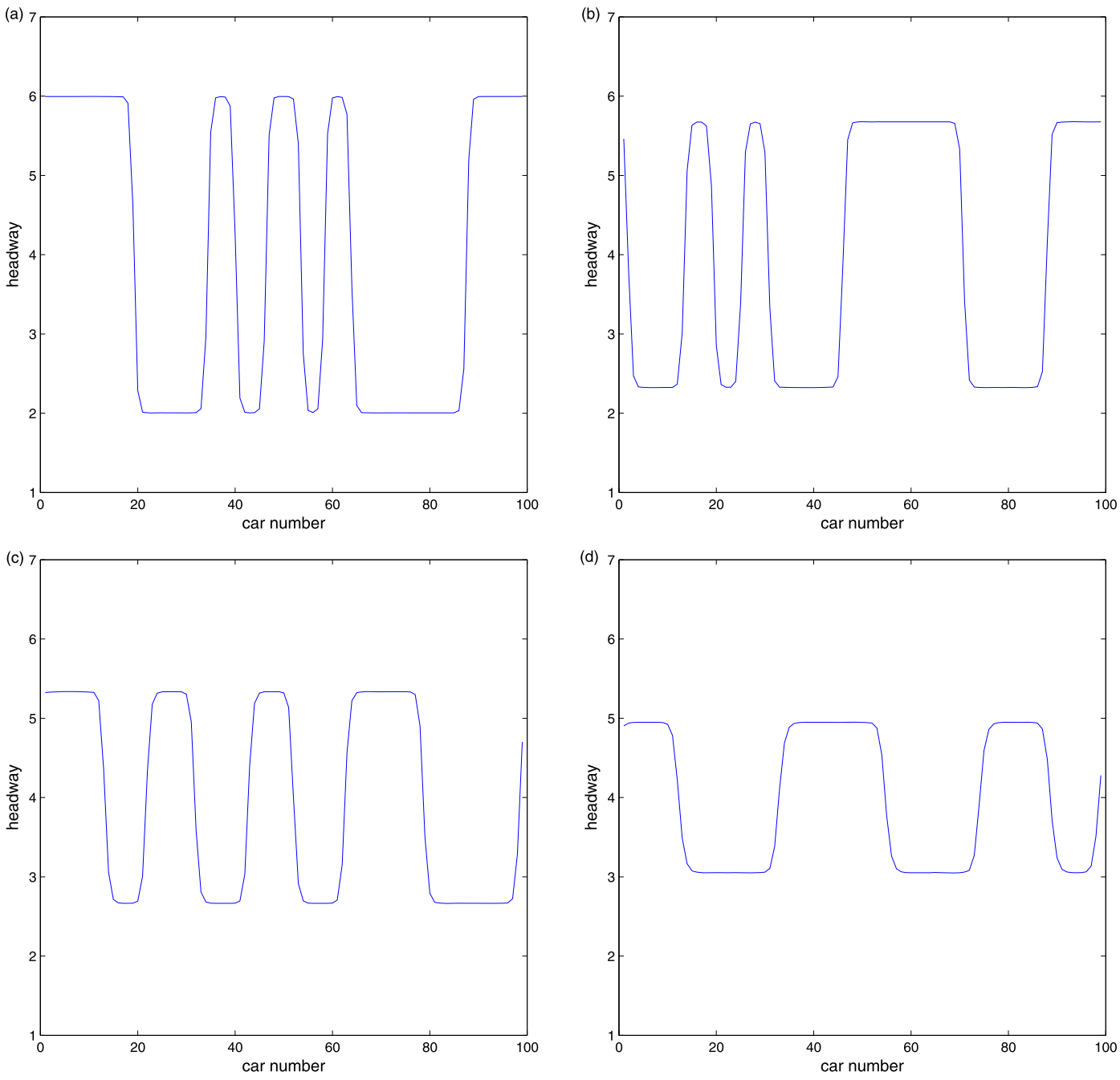

Fig. 5. Headway profile of the density wave at $t = 10080$ correspond to Fig. 4, respectively.

The amplitude C of the kink–antikink solution (22) is given by

$$C = \sqrt{\frac{g_1 B}{g_2}\left|\frac{a_c}{a} - 1\right|}.$$

The kink solution represents the coexisting phase, which consists of the freely moving phase with low density and the jammed (or congested) phase with high density phase. The headways of the freely moving phase and the jammed phase are given, respectively, by $\Delta x = h_c + C$ and $\Delta x = h_c - C$. Thus, we obtain the coexisting curve in the $(\Delta x, a)$ plane (see Fig. 1).

Thus, the mKdV equation is derived around the critical point and the kink–antikink density wave appears in the unstable region. In Section 5, through numerical simulations, the kink–antikink waves appear many times. When $\tau_1 = \tau_2 = 0$, the results given in this section agree with the results given in Ref. [23].

5. Numerical simulations

To verify the theoretical results, we carry out numerical simulations for the FVD-Ds model described by Eq. (2) under the periodic boundary condition. The impact of local small disturbances to the system with two different time delays is investigated. The uniform flow is such that the vehicles move with the constant headway 4.0 and the initial conditions are chosen as follows

$$\Delta x_n(0) = 4.0 \quad (n \neq 50, 51), \qquad \Delta x_n(0) = 4.0 - 0.1 \quad (n = 50),$$
$$\Delta x_n(0) = 4.0 + 0.1 \quad (n = 51),$$

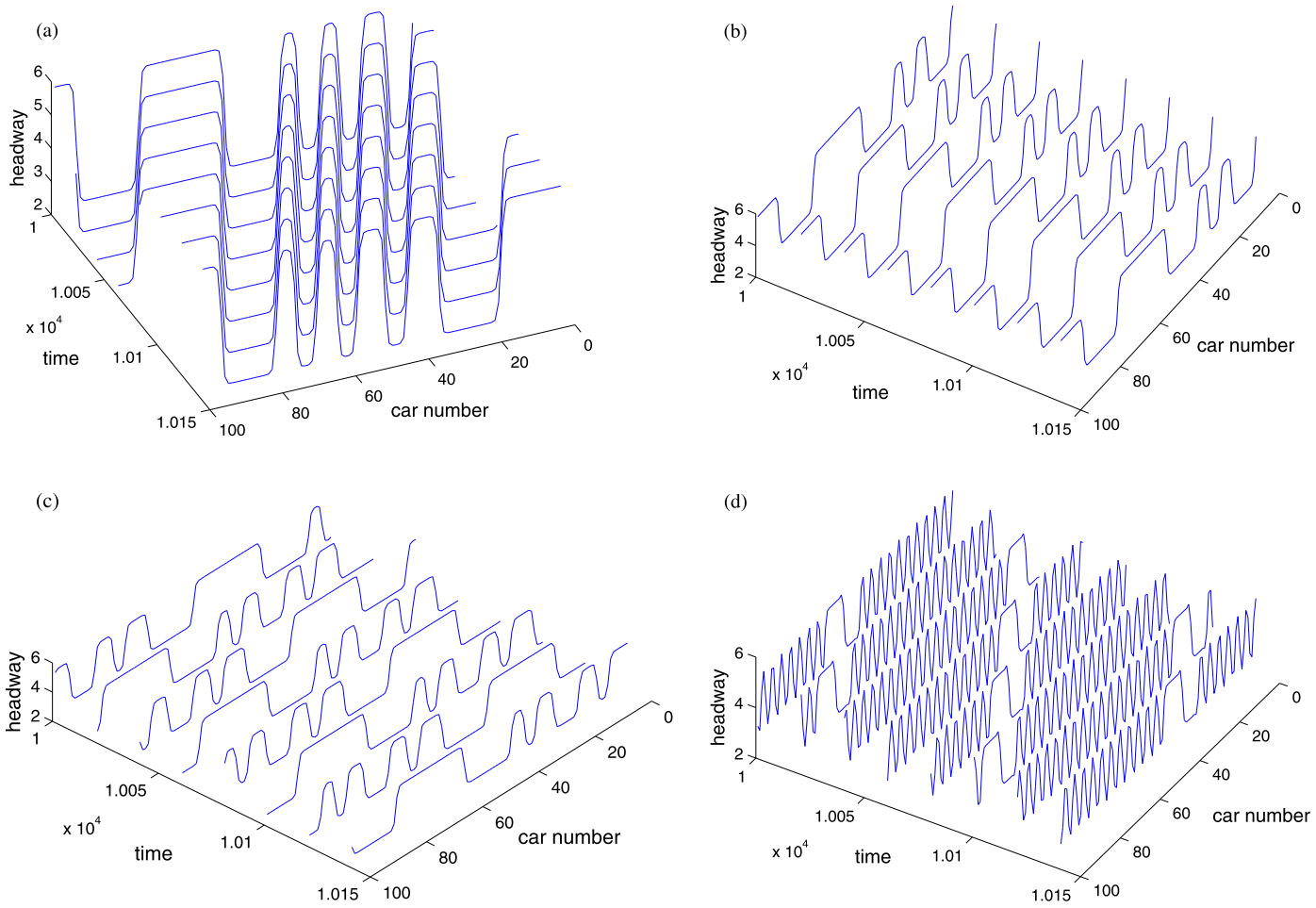

Fig. 6. Space–time evolution of the headway with $\tau_1 = 0.3$ and different τ_2 after $t = 10\,000$ ($a = 2.0$).

where the total number of cars is $N = 100$, the safety distance is $h_c = 4.0$, $v_{\max} = 3$, $\lambda = 0.2$.

Fig. 2 shows the typical traffic patterns after a sufficiently long time $t = 10^4$ with different τ_1 and τ_2 for $a = 2.95$. According to the process of sensing the headway and velocity between the leader and follow car [32,39], we find that the time delay of headway should be larger than that of velocity. In Fig. 2, the patterns (a), (b), (c) and (d) exhibit the time evolution of the headway for $\tau_1 = 0.4, \tau_2 = 0.1$; $\tau_1 = 0.3, \tau_2 = 0.1$; $\tau_1 = 0.2, \tau_2 = 0.1$ and $\tau_1 = 0.1, \tau_2 = 0.1$, respectively. By using the stability condition (8), the traffic flow patterns (a), (b) and (c) are unstable and the traffic flow pattern (d) is stable. In patterns (d) the density waves disappear and the traffic flow is uniform over the whole space. This means the traffic will become stable when the difference between τ_1 and τ_2 decreases. This phenomenon coincides with the stability analysis in Section 3.

Fig. 3 shows the headway profile obtained at $t = 10\,080$ corresponding to Fig. 2, respectively.

Fig. 4 shows the typical traffic patterns in the unstable region after a sufficiently long time $t = 10^4$ with different reaction-time delays for $a = 2.0$. The patterns (a), (b), (c) and (d) exhibit the time evolution of the headway for $\tau_1 = 0.4, \tau_2 = 0.1$; $\tau_1 = 0.3, \tau_2 = 0.1$; $\tau_1 = 0.2, \tau_2 = 0.1$ and $\tau_1 = 0.1, \tau_2 = 0.1$, same as Fig. 2. Because the stability condition (8) is not satisfied, the traffic flow is unstable in patterns (a)–(d). But we find that the amplitude of the density wave decreases as the difference between τ_1 and τ_2 decreases. These patterns are the stop-and-go traffic jams in real traffic.

Fig. 5 shows the headway profile obtained at $t = 10\,080$ corresponding to Fig. 4, respectively.

Fig. 6 shows the typical traffic patterns after a sufficiently long time $t = 10^4$ with different τ_1 and τ_2 for $a = 2.0$. In Fig. 6, the patterns (a), (b), (c) and (d) exhibit the time evolution of the headway for $\tau_1 = 0.3, \tau_2 = 0.0$; $\tau_1 = 0.3, \tau_2 = 0.1$; $\tau_1 = 0.3, \tau_2 = 0.2$ and $\tau_1 = 0.3, \tau_2 = 0.3$. By using the stability condition (8), all the traffic flow patterns are unstable. Traffic flow become more stable when the difference between τ_1 and τ_2 decreases. This coincides with the results getting from other figures. Especially, the traffic flow is more unstable when $\tau_1 = 0.3$ and $\tau_2 = 0.0$ comparing with other cases.

Fig. 7 shows the headway profile obtained at $t = 10\,080$ corresponding to Fig. 6, respectively.

These numerical results are very sensitive to the choice of a. Figs. 2, 4 and 6 indicate that the decrease of the difference between τ_1 and τ_2 leads to the disappearance of perturbation when a is in a special domain. Although the traffic flow is unstable to different sets of τ_1 and τ_2, the amplitude of density waves decrease as the difference between τ_1 and τ_2 decreases. This indicates that traffic jams will be worse when there are large differences of the two delays.

From Fig. 2 to Fig. 7, we see that the kink–antikink density waves, the solution of mKdV equation, appear as traffic jams and they propagate backwards.

After a sufficiently long time, the traffic state is close to stationary where the motions of vehicles organize hysteresis loops in the headway-velocity space as shown in Fig. 8. Changing the

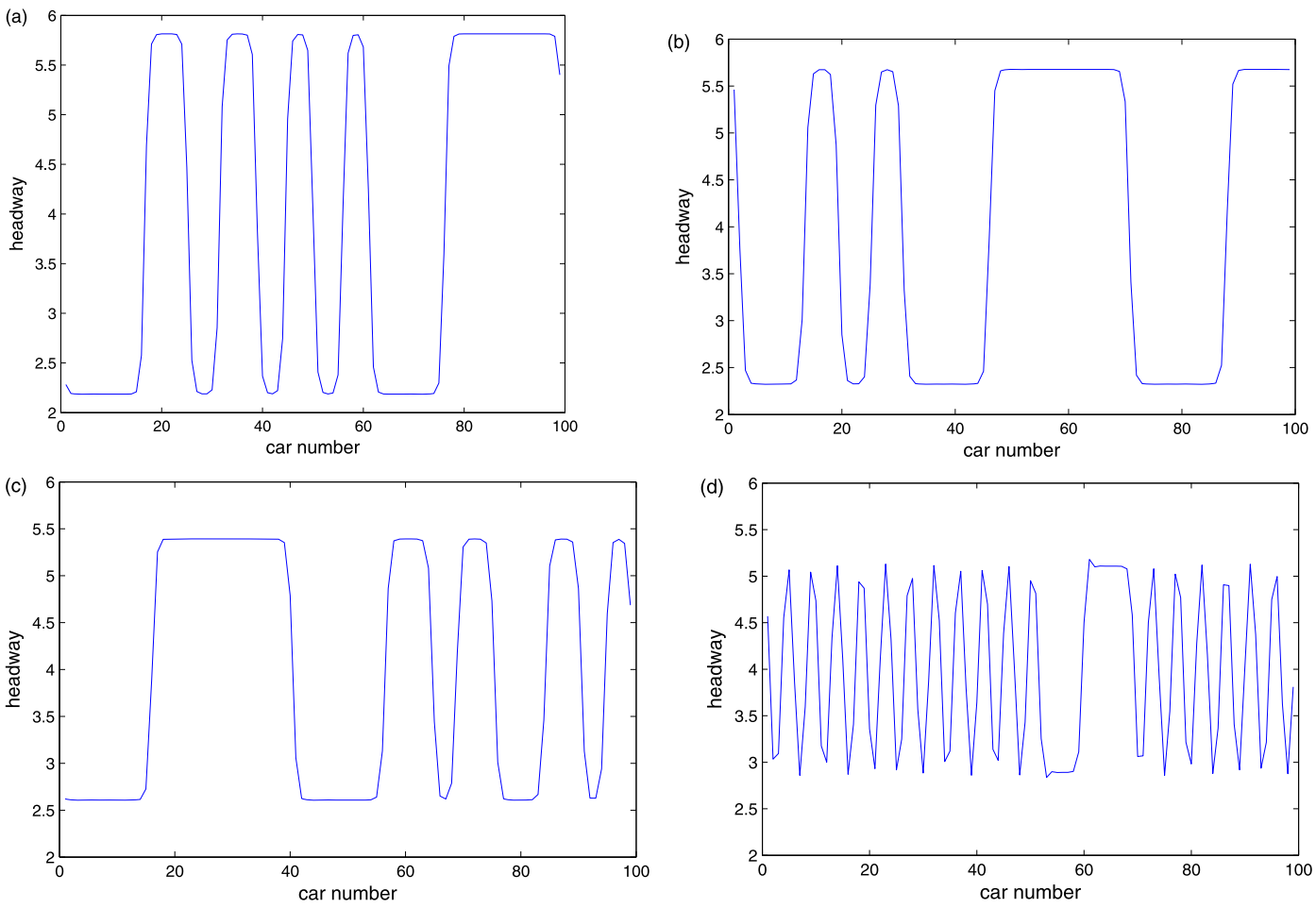

Fig. 7. Headway profile of the density wave at $t = 10080$ correspond to Fig. 6, respectively.

values of τ_1 and τ_2, loops of different sizes are obtained. When $\tau_1 = \tau_2 = 0.1$, there is only a black point on the optimal velocity curve but there is not a hysteresis loop because the stability condition is held and the traffic flow is stable. Comparing with the hysteresis loops for FVD model without delay at different values of λ, the hysteresis loops of FVD-Ds model have no the negative velocities [4].

6. Summary

The time delay is a critical parameter to the dynamical traffic flow's study. In this paper, we present an extended FVD model by taking into account two different time delays in sensing headway and velocity. These two delays have important effects upon the property of the traffic flow, especially the stability condition. The stability analysis shows that decreasing the difference between two time delays leads to the stabilization of the traffic flow. The evolution of traffic jams described by the mKdV equation is derived by using the reductive perturbation method. The numerical results show that traffic jams are suppressed efficiently when the difference of two time delays in sensing headway and velocity decreases. Traffic flow is more stable with two delays in sensing headway and velocity than the case with only one delay in sensing headway. This confirms the fact that time delays are critical parameters to the dynamical traffic flow study. The numerical analysis also studies the impact of local small disturbance to the system.

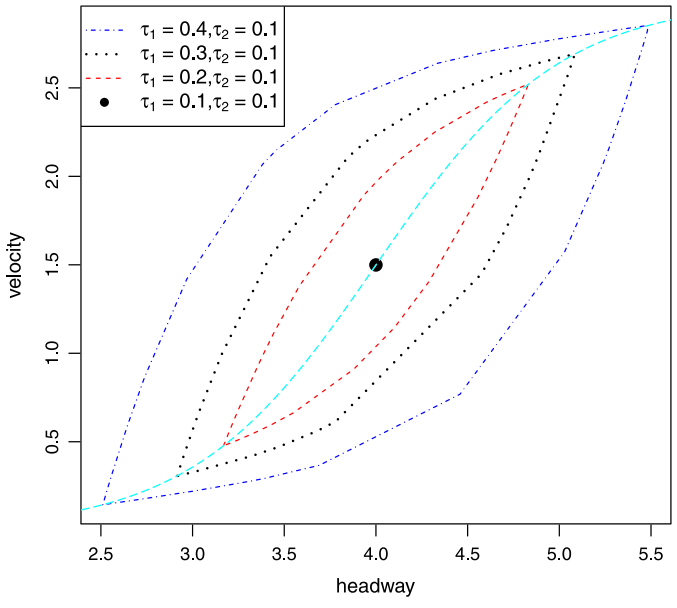

Fig. 8. Hysteresis loops for different delays ($a = 2.95$).

Acknowledgements

This work is supported by National Natural Science Foundation of China (Grant No. 11102165), Natural Science Foundation

of Shaanxi Province (2013JQ7014, 2012JM1001), the new direction of the Young Scholar of Northwestern Polytechnical University and Foundation for Fundamental Research of Northwestern Polytechnical University (JC20110265).

References

[1] L.A. Pipes, J. Appl. Phys. 24 (1953) 274.
[2] M. Bando, K. Hasebe, A. Nakayama, A. Shibata, Y. Sugiyama, Phys. Rev. E 51 (1995) 1035.
[3] D. Helbing, B. Tilch, Phys. Rev. E 58 (1998) 133.
[4] R. Jiang, Q.S. Wu, Z.J. Zhu, Phys. Rev. E 64 (2001) 017101.
[5] B.S. Kerner, S.L. Klenov, J. Phys. A, Math. Gen. 39 (2006) 1775.
[6] K. Nagel, M. Schreckenberg, J. Phys. I 2 (1992) 2221.
[7] S. Tadaki, M. Kikuchi, Phys. Rev. E 50 (1994) 4564.
[8] B.H. Wang, Y.R. Kwong, B. Hu, Phys. Rev. E 60 (1999) 149.
[9] N. Moussa, A.K. Daoudia, Eur. Phys. J. B 31 (2003) 413.
[10] T. Nagatani, Physica A 388 (2009) 1673.
[11] Q.L. Li, B.H. Wang, M.R. Liu, Physica A 390 (2011) 1356.
[12] M. Fukui, Y. Ishibashi, K. Nishinari, Physica A 392 (2013) 902.
[13] D. Helbing, Phys. Rev. E 53 (1996) 2366.
[14] D. Helbing, Rev. Mod. Phys. 73 (2001) 1067.
[15] H.K. Lee, H.W. Lee, D. Kim, Phys. Rev. E 69 (2004) 016118.
[16] T. Li, Physica D 207 (2005) 41.
[17] T. Li, Netw. Heterog. Media 3 (2013) 8.
[18] R. Jiang, M.B. Hu, B. Jia, R.L. Wang, Q.S. Wu, Phys. Lett. A 365 (2007) 6.
[19] M. Dolfin, Appl. Math. Lett. 25 (2012) 2162.
[20] Y.R. Kang, D.H. Sun, Nonlinear Dyn. 71 (2013) 531.
[21] T.S. Komatsu, S.I. Sasa, Phys. Rev. E 52 (1995) 5574.
[22] M. Muramatsu, T. Nagatani, Phys. Rev. E 60 (1999) 180.
[23] Z.H. Ou, S.Q. Dai, L.Y. Dong, J. Phys. A, Math. Gen. 39 (2006) 1251.
[24] L. Yu, Z.K. Shi, B.C. Zhou, Commun. Nonlinear Sci. Numer. Simul. 13 (2008) 2167.
[25] T. Nagatani, Rep. Prog. Phys. 65 (2002) 1331.
[26] R. Sipahi, F.M. Atay, S.I. Niculescu, SIAM J. Appl. Math. 68 (2007) 738.
[27] R.E. Chandler, R. Herman, E.W. Montroll, Oper. Res. 7 (1958) 165.
[28] M. Bando, K. Hasebe, K. Nakanishi, A. Nakayama, Jpn. J. Ind. Appl. Math. 17 (2000) 275.
[29] L.C. Davis, Physica A 319 (2003) 557.
[30] G. Orosz, R.E. Wilson, B. Krauskopf, Phys. Rev. E 70 (2004) 026207.
[31] G. Orosz, B. Krauskopf, R.E. Wilson, Physica D 211 (2005) 277.
[32] R. Sipahi, S.I. Niculescu, in: Proceedings of 6th IFAC Workshop on Time Delay Systems, L'Aquila, Italy, 2006, p. 187.
[33] M. Treiber, A. Kesting, D. Helbing, Transp. Res. Rec. 1999 (2007) 23.
[34] H.B. Zhu, S.Q. Dai, Physica A 387 (2008) 3290.
[35] H.X. Ge, X.P. Meng, R.J. Cheng, S.M. Lo, Physica A 390 (2011) 3348.
[36] L. Yu, T. Li, Z.K. Shi, Physica A 389 (2010) 2607.
[37] G. Orosz, R.E. Wilson, R. Szalai, G. Stepan, Phys. Rev. E 80 (2009) 046205.
[38] H.X. Ge, R.J. Cheng, S.Q. Dai, Physica A 357 (2005) 466.
[39] D.L. Gerlough, M.J. Huber, Traffic flow theory, Special Report 165, Transportation Research Board, National Research Council, Washington, DC, 1975.